Published in final edited form as:

Cancer Res. 2015 April 1; 75(7): 1356–1365. doi:10.1158/0008-5472.CAN-14-1540.

Treatment of invasive brain tumors using a chain-like nanoparticle

Pubudu M. Peiris[1,2,3], **Aaron Abramowski**[3,4], **James Mcginnity**[1,3], **Elizabeth Doolittle**[1,2,3], **Randall Toy**[1,2,3], **Ramamurthy Gopalakrishnan**[2,3], **Shruti Shah**[1,3], **Lisa Bauer**[2,3,5], **Ketan B. Ghaghada**[6,7], **Christopher Hoimes**[8,9], **Susann M. Brady-Kalnay**[9,10], **James P. Basilion**[1,2,3,9], **Mark A. Griswold**[2,3,9], and **Efstathios Karathanasis**[1,2,3,9,*]

[1] Department of Biomedical Engineering, Case Western Reserve University, Cleveland, Ohio

[2] Department of Radiology, Case Western Reserve University, Cleveland, Ohio

[3] Case Center for Imaging Research, Case Western Reserve University, Cleveland, Ohio

[4] Department of Biochemistry, Case Western Reserve University, Cleveland, Ohio

[5] Department of Physics, Case Western Reserve University, Cleveland, Ohio

[6] Edward B. Singleton Department of Pediatric Radiology, Texas Children's Hospital, Houston, Texas

[7] Department of Radiology, Baylor College of Medicine, Houston, Texas

[8] University Hospitals Case Medical Center, Cleveland, Ohio

[9] Case Comprehensive Cancer Center, Case Western Reserve University, Cleveland, Ohio

[10] Department of Molecular Biology and Microbiology, Case Western Reserve University, Cleveland, Ohio

Abstract

Glioblastoma multiforme is generally recalcitrant to current surgical and local radiotherapeutic approaches. Moreover, systemic chemotherapeutic approaches are impeded by the blood-tumor barrier. To circumvent limitations in the latter area, we developed a multicomponent, chain-like nanoparticle that can penetrate brain tumors, composed of three iron oxide nanospheres and one drug-loaded liposome linked chemically into a linear chain-like assembly. Unlike traditional small molecule drugs or spherical nanotherapeutics, this oblong-shaped, flexible nanochain particle possessed a unique ability to gain access to and accumulate at glioma sites. Vascular targeting of nanochains to the $\alpha_v\beta_3$ integrin receptor resulted in a 18.6-fold greater drug dose administered to brain tumors than standard chemotherapy. By two hours after injection, when nanochains had exited the blood stream and docked at vascular beds in the brain, the application of an external low-power radiofrequency field was sufficient to remotely trigger rapid drug release. This effect was produced by mechanically induced defects in the liposomal membrane caused by the

* Author to whom correspondence should be addressed: Efstathios Karathanasis, 2071 Martin Luther King Jr. Drive, Wickenden Building, Cleveland, Ohio 44106, USA, Phone: +1-216-844-5281; Fax: +1-216-844-4987; stathis@case.edu.

Conflicts of interest: The authors disclose no potential conflicts of interest.

oscillation of the iron oxide portion of the nanochain. In vivo efficacy studies conducted in two different mouse orthotopic models of glioblastoma illustrated how enhanced targeting by the nanochain facilitates widespread site-specific drug delivery. Our findings offer preclinical proof of concept for a broadly improved method for glioblastoma treatment.

Keywords

Nanochains; invasive brain tumor; targeting glioma; radiofrequency-triggered drug release; chemotherapy

INTRODUCTION

The invasive forms of brain tumor, such as glioblastoma multiforme (GBM) are terminal upon diagnosis and no new protocols have been developed in more than 30 years. Current approaches for the treatment of glioma are limited in their effectiveness, because GBM tumors are characteristically diffuse, highly invasive, non-localized, and drug penetration across the blood-tumor barrier (BTB) is poor for most chemotherapeutic agents (1, 2). Today, systemic chemotherapy is not the primary treatment of choice for brain tumors due to the presence of the BTB. In an effort to avoid having to penetrate the BTB, implantable biodegradable drug depots within a brain tumor are currently being used in clinical practice to localize a chemotherapeutic and allow for controlled drug delivery (3). However, this method relies on drug diffusion from a central core. As a result, drug usually cannot reach the tumor periphery where the most aggressive cells persist. Therefore, the ideal drug delivery system should be based on systemic intravascular administration, which utilizes the tumor's own blood supply for transport allowing for drug delivery throughout the tumor and its invasive sites.

Notably, nanoparticles have shown promise, because they can be designed not only to carry a range of cytotoxic drugs, but also to "smuggle" the drug into intracranial tumors such as gliomas. For example, while the potent chemotherapeutic drug doxorubicin (abbreviated as DOX) exhibits insignificant penetration of the BTB, it was demonstrated in patients with glioblastomas that long circulating liposomal nanoparticles containing DOX achieved a 13-19-fold higher accumulation of DOX in brain cancerous lesions compared to the normal brain (4). However, even though the BTB compromises the impermeable nature of the blood-brain barrier (BBB), blood vessels are not nearly as leaky as the angiogenic vessels observed in other cancer types (5). Thus, nanoparticles exhibit relatively low penetration into gliomas with a patchy, near-perivascular distribution resulting in failure to deliver drugs to the difficult-to-reach invasive sites of brain tumors (6).

To circumvent the limitations of today's drugs in treating invasive brain tumors, a multicomponent, flexible chain-like nanoparticle was developed. The nanoparticle, termed nanochain, is comprised of three iron oxide (IO) nanospheres and one drug-loaded liposome chemically linked into a linear, chain-like assembly (Fig. 1A,B) (7, 8). The multicomponent nature and shape of the particle result in two unique features that facilitate effective treatment of difficult-to-treat brain tumors using a low dose of cytotoxic drugs as illustrated in Fig. 1C (7, 9, 10). Contrary to traditional small-molecule drugs or more contemporary

nanotherapeutics, the nanochain particle possesses a unique ability to gain rapid access to and be deposited at brain tumor sites. The nanochains are capable of transporting their drug cargo to brain tumors *via* highly specific vascular targeting of the vascular bed associated with the primary tumor mass and its invasive sites. Numerous studies have shown that $\alpha_v\beta_3$ integrin is highly overexpressed on brain tumors' vascular bed, which has led to clinical trials testing integrin antagonists as antiangiogenic agents for GBM patients (11-16). Furthermore, $\alpha_v\beta_3$ integrin is minimally expressed on normal resting blood vessels (17, 18). Notably, RGD-targeted nanoparticles are rapidly internalized by endothelial cells *via* the $\alpha_v\beta_3$ integrin receptor (13, 14, 19, 20). Hence, the nanochain utilizes a cyclic RGD peptide as a ligand to target the $\alpha_v\beta_3$ integrin receptor on the endothelium of angiogenic blood vessels of brain tumors. The size, shape and flexibility of the nanochains significantly increase the margination of the particles towards the blood vessel walls in microcirculation (*i.e.*, continuous scavenging of vascular walls), and targeting avidity of nanoparticles (*i.e.*, latching on vascular target) due to geometrically enhanced multivalent attachment on the vascular target (9).

However, even after successful targeting to brain tumors, the drug molecules must spread to all the cancer cells, especially the hard-to-reach ones, resulting in widespread anticancer activity throughout the entire volume of tumors. While nanoparticles typically release their content slowly, drug release from nanochains can be remotely triggered due to mechanically induced defects of the liposomal membrane caused by the oscillation of the IO portion of the nanochain in the presence of an RF field (7). Two hours later, after nanochains slip from the blood stream and dock on the vascular bed of brain tumors, a low-power radiofrequency (RF) field (10 kHz frequency, 5 mT amplitude) is applied outside the body. The field causes the nanochain to vibrate, breaking open the drug-loaded liposome and spreading cytotoxic drugs to the entire volume of glioma sites (7, 21).

In contrast to delivery of cancer drugs *via* passive intratumoral accumulation, our strategy utilizes the overexpressed $\alpha_v\beta_3$ integrin receptor as a docking site to establish well-distributed drug reservoirs on the brain tumor vasculature, which can subsequently spread free drug in the tumor interstitium using an RF field as an external trigger. In this study, we show that the synergy of nanochain's enhanced targeting and widespread drug delivery capabilities facilitates enhanced treatment of brain tumor sites, which are otherwise inaccessible by conventional therapies.

MATERIALS AND METHODS

Materials

The primary antibody for the specific endothelial antigen CD31 was purchased from BD Biosciences Pharmingen (San Diego, CA). Secondary antibodies and cell culture media were obtained from Invitrogen (Carlsbed, CA). Cross-Linked Ethoxylate Acrylate Resin (CLEAR) resin, reaction vessels, other accessories for solid-phase chemistry and the cyclo (Arg-Gly-Asp-D-Phe-Cys) or c(RGDfC) peptide were purchased from Peptides International Inc (Louisville, KY). The crosslinkers 3,3′-Dithiobis(sulfosuccinimidylpropionate) (DTSSP) and sulfosuccinimidyl 4-[N-maleimidomethyl]cyclohexane-1-carboxylate (sulfo-SMCC), and the cleaving agent Tris[2-

carboxyethyl] phosphine (TCEP) were obtained from Thermo Fisher Scientific (Cleveland, OH). Polyethylene glycol (PEG) conjugates were purchased from Laysan Bio (Arab, AL). General solvents and chemicals were obtained from Thermo Fisher Scientific (Cleveland, OH). Doxorubicin (DOX) was obtained from Sigma (Saint Louis, MO).

Synthesis and characterization of nanoparticles

The nanochains were fabricated using a two-step solid-phase chemistry based on a previously published method (7, 8). More detailed on the synthesis of the nanochain particles can be found in previous publications (7, 8, 21).

Tumor model

All animal procedures were conducted under a protocol approved by the IACUC of Case Western Reserve University. The CNS-1 rodent glioma tumor model was used for these studies. Five- to 8-week-old NIH athymic nude mice (20–25 g each) were housed in the Athymic Animal Core Facility at Case Western Reserve University according to institutional policies. CNS-1 cells were infected with green fluorescent protein (GFP) encoding lentivirus, harvested for intracranial implantation by trypsinization, and concentrated to 1×10^5 cells/μL in PBS. Mice were anesthetized by intraperitoneal administration of 50 mg/kg ketamine/xylazine and fitted into a stereotaxic rodent frame. Cells were implanted at AP= +0.5 and ML= − 2.0 from bregma at a rate of 1 μL/min in the right striatum at a depth of −3 mm from dura. A total of 200,000 cells were implanted per mouse. Similar procedures were employed for the 9L glioma model.

Histological evaluation

Once the appropriate tumor sizes were established (~8 days after tumor inoculation), the animals were injected intravenously with the nanochain particles at a dose of 0.5 mg/kg DOX. At 2 h after injection, the animals were exposed to the RF field for 60 min. Animals were euthanized 24 h after injection, and organs were extracted and analyzed histologically for location of brain tumor (CNS-1-GFP cells). Serial tissue sections of 12-μm thickness were stained for the specific endothelial antigen CD31 and with the nuclear stain DAPI. The tissue sections were imaged at 5, 10 and 20x magnification on the Zeiss Axio Observer Z1 motorized FL inverted microscope. To evaluate the spread of drugs in relation to the location of nanochains, we used Prussian blue to stain iron. Direct fluorescence (red) imaging was used for DOX. Histological sections were imaged on a Zeiss Axio Observer Z1 motorized FL inverted microscope. In order to obtain an image of the entire section, a montage of each section was made using the automated tiling function of the microscope.

Survival study

Once the tumors were established (~five days; histologically confirmed), the animals were injected intravenously with the nanochain at a dose of 0.5 mg/kg DOX. At 2 h after injection, a 60-min application of the RF field (amplitude B=2 mT, frequency f=10 kHz, RF power=3-5 Watts) was employed using a custom-made solenoid (N=105 turns, Inner Diameter=2.8 cm) (7). During this procedure the animals were anesthetized through the administration of inhalant isoflurane. Two subsequent treatments were applied at time

intervals of two days at the same DOX dose followed by exposure to RF following identical protocol to the first cycle (if applicable). Following the same schedule for the treatments and RF application, control groups included animals treated with nanochains (no RF), liposomal DOX with RF, free DOX, and saline. After tumor inoculation, mice were monitored daily for any abnormal symptoms. The well-being of the animals took priority in decisions regarding euthanasia or other interventions. When animals showed a 10% loss of body weight, they were euthanized in a CO_2 chamber. While the 10% weight loss was the primary endpoint criterion for the vast majority of the animals, two animals in the CNS-1 glioma model, one animal in the DOX-treated group and one animal in the nanochain-treated group (+RF), had to be euthanized because the animals suffered from inactivity and lethargy. At the terminal point, the tumor mass at the primary site had grown significantly with a final size of about 1.8 mm. While the final size of the tumor at the primary site does not indicate the degree of tumor invasiveness, we histologically observed a considerable number of distant sites with dispersive brain tumor cells in the case of the CNS-1 glioma model. Time of death was determined to be the following day.

Statistical analysis

Means were determined for each variable in this study and the resulting values from each experiment were subjected to one-way analysis of variance with post hoc Bonferroni test (SPSS 15, Chicago, IL). A P value of less than 0.05 was used to confirm significant differences. Normality of each data set was confirmed using the Anderson-Darling test.

RESULTS

Synthesis and characterization of nanochains

To fabricate the multicomponent nanochain particles, a stepwise solid-phase chemistry approach was developed. In the first step (Fig. 2A), amine-PEG functionalized IO nanospheres (hydrodynamic diameter of 27 nm) were conjugated onto amine-functionalized CLEAR resin *via* a homobifunctional crosslinker reactive towards primary amines containing a disulfide bridge. The IO nanospheres were allowed to bind to the solid support and then cleaved off using a reducing agent. The thiolytic cleavage liberated the IO nanosphere from the solid support converting the amines to a different chemical functionality (thiol group) on the portion of the nanosphere's surface that was linked to the resin. The second step (Fig. 2B) employed the same type of resin and the modified nanospheres were introduced in a step-by-step manner using a heterobifunctional crosslinker for conjugation between primary amine and sulfhydryl groups. As a final component, an amine functionalized DOX-loaded liposome with a hydrodynamic diameter of 35 nm was added. It should be noted that each step included multiple washing cycles to remove any unbound nanospheres and excess reagents from the nanoparticle-resin complex. In the end, the thiol of the cysteine residue of the c(RGDfC) peptide was used to conjugate the targeting ligand to the remaining amine-terminated PEG on the surface of nanochains. Finally, the $\alpha_v\beta_3$ integrin-targeting nanochains were cleaved off the resin and recovered.

Due to the simplified purification procedure and easy handling of multiple reaction vessels, the solid-phase-based synthesis enables us to manufacture large amounts of nanochains that

exhibited a high degree of uniformity. Based on analysis of multiple TEM images (minimum count was 200 particles), the majority of the particles (>85%) is comprised of nanochains with 3 IO spheres and 1 liposome (7, 21). As shown in Fig. 2C, the hydrodynamic size of the nanochain particle and each constituent nanosphere, as measured by dynamic light scattering (DLS), verified the TEM findings. Due to the high intraliposomal space available for drug encapsulation and the efficient remote loading technique (22), the entrapment efficiency was very high (drug cargo: 6.8×10^{-5} ng DOX per particle). To determine the contribution of blood plasma to leakage of DOX, Fig. 2D shows an *in vitro* stability test. The dialysis curve plateaued after ~3 h, and the nanochain exhibited a leakage of ~6.5% of the total encapsulated DOX after 24 h, which was comparable to the leakage of a typical 100-nm liposome.

Vascular targeting of brain tumors

To evaluate the nanochain's ability at targeting brain tumors, we compared the $\alpha_v\beta_3$ integrin-targeting nanochains to $\alpha_v\beta_3$ integrin-targeting 30-nm liposomes, their non-targeting variant, and free DOX. For this study, we selected the orthotopic CNS-1 glioma model. Recent reviews have compared the most commonly used rodent glioma models (*e.g.*, C6, 9L) in terms of pathological and genetic similarities to the human disease (23, 24). The CNS-1 model is one of the few models that recapitulate the microenvironment of the human disease and displays several histological features and diffuse growth and invasive pattern similar to human glioblastoma multiforme (GBM). In addition to their ability to express several glioma markers, a three-dimensional cryo-imaging technique showed that the rodent CNS-1 glioma cells is a valid system to study the highly dispersive nature of glioma tumor cells along blood vessels and white matter tracts *in vivo* (25).

The animals were injected with the various DOX formulations *via* tail vein at a dose of 0.5 mg/kg DOX 8 days after orthotopic tumor inoculation. The animals were transcardially perfused with heparinized PBS 24 h after intravenous administration, and brains were retrieved and analyzed for DOX content following an established protocol (26). At this time point, DOX was undetectable in blood circulation. We predominantly collected the tumor mass at the primary site, because it was very challenging to identify the margins of the invasive sites of the tumor. Vascular targeting of nanochains resulted in a 4.7% of the administered dose being localized in brain tumor (Fig. 3A), which was 18.6-fold higher than free DOX. Free DOX and nontargeted liposomes exhibited very low accumulation (<1% of injected dose) at brain cancer sites. The targeted liposomes and nontargeted nanochains displayed an accumulation of 1.45 and 1.75% of the injected dose, respectively, in brain tumors. As expected, the levels of DOX in normal brain were undetectable in the case of all the formulations.

After evaluating the significant targeting enhancement of DOX to brain tumors using nanochains, we used non-invasive imaging to assess the therapeutic efficacy of the nanoparticle with or without the RF application. By infecting the CNS-1 cells with green fluorescent protein (GFP) encoding lentivirus, the expression of GFP of the CNS-1 cells enabled *in vivo* imaging using a Maestro fluorescence imaging system (Supplementary Fig. S1A). As a metric of the response of brain tumors to various treatments (n=5 in each group),

quantification of fluorescence signal was used (Fig. 3B). Due to the emission of GFP in the green zone of the visible spectrum, the depth-dependent attenuation of the fluorescence signal primarily by the skull (and the brain tissues) does not allow accurate quantification of the number of CNS-1 glioma cells in the case of *in vivo* imaging (Supplementary Fig. S1B). However, the relative differences of fluorescence signal among the various treatments can be used as a comparison in a semi-quantitative manner. At 8 days after orthotopic tumor inoculation, the animals were intravenously injected with nanochains at a dose of 0.5 mg DOX per kg of body weight. A 60-min application of the RF field (amplitude B=5 mT, frequency f=10 kHz) was employed at the point of maximum accumulation of the nanochain in brain tumors (2 h after injection) (7). Previous *in vitro* studies identified that a 60-min application of the RF field at the selected operating conditions guarantees ~100% release of nanochain's drug cargo (7). Maestro imaging was performed before and 48 h after injection to allow for the cytotoxic effects of DOX to occur. Fig. 3B shows that the signal of the untreated animals doubled within 48 h. While free DOX decelerated the disease, the brain tumor continued growing as indicated by the increase of fluorescence signal. Even with the nanochain's enhanced targeting efficacy, the nanochain therapy (without RF) resulted in a similar anticancer effect to free DOX. However, animals treated with nanochain followed by application of the RF field exhibited a substantial decrease of fluorescence signals, which indicates the additional therapeutic effects of the RF-triggered release. Furthermore, no temperature increase of the brain tissue was observed due to the RF field (Supplementary Fig. S2), indicating that the triggered release mechanism of drug from the nanochains is not based on hyperthermia.

Histological evaluation

After evaluating the targeting capabilities and anticancer effects of the nanochain in a macroscopic manner, we assessed the localization of nanochain in invasive glioma and the degree and topology of DOX delivery with or without the application of the RF field. Histological analysis was performed on separate groups of mice 24 h after injection (n=3). A representative image of a brain section is shown in Fig. 4A (left panel) displaying the presence of the primary tumor and clusters of invasive cancer cells dispersed in the brain. Bright field microscopy of the same histological section stained with Hematoxylin-Eosin is shown in Supplementary Fig. S3. Most notably, application of the RF field resulted in widespread delivery of DOX at both the primary and invasive sites of brain tumor (right panel of Fig. 4A). We then focuses on an invasive site (shown by the yellow circle in Fig. 4A) to assess the ability of the nanochain to deliver drugs to dispersing glioma cells. Imaging at higher magnification of this invasive site showed that nanochains were selectively localized on the endothelium associated with cancerous sites (left panel in Fig. 4B). Notably, application of the RF field facilitated the spreading of DOX at distant cells away from nanochain deposits (right panel in Fig. 4B). While the RF-triggered release resulted in widespread delivery of DOX to the target site (Fig. 4C), no spread of DOX was observed in the case of nanochain-treated animals that were not exposed to RF, since the fluorescence signal of intraliposomal DOX is quenched (Fig. 4D). The *in vivo* anticancer effects of the nanochain treatment followed by RF observed in histology are consistent to cell cytotoxicity studies (Supplementary Fig. S4). While 30-nm liposomal DOX, 100-nm liposomal DOX and nanochain without RF exhibited moderate cytotoxicity (less than 30%

relative cytotoxicity), RF-triggered release of DOX from nanochain had significant cytotoxic effects (65% cytotoxicity), which was comparable to the effect of free DOX (75% cytotoxicity) indicating the release of free DOX molecules from the nanochain particles upon application of the RF field.

Survival studies

The therapeutic effect of the nanochain treatment was determined in two orthotopic glioma models by measuring survival times. Control treatments included free DOX followed by RF and nanochain without RF. The treatments were administered three times (Fig. 5A), each at a dose of 0.5 mg/kg DOX. Targeted nanochains exhibited a 2.6, 3.2 and 6-fold higher deposition in brain tumors than nontargeted nanochains, targeted liposomes and nontargeted liposomes, respectively (Fig. 5B). Since the targeting efficiency of the nanochains to brain tumors was found to be significantly higher than those formulations, we chose to only assess the effect of targeted nanochains with or without the combination of the RF field on the survival rate. Not surprisingly, the free DOX treatment had negligible therapeutic benefits in the CNS-1 model. On the other hand, even with their enhanced targeting capability, nanochains (without RF) exhibited a moderate effect. However, the survival time of the nanochain-treated animals followed by RF was significantly increased (25±3 days; mean ±s.d.) when compared to the nanochain-treated group without RF (16±1 days), DOX-treated group (10±3 days), and the untreated group (9±1 days). In comparison to standard chemotherapy (*i.e.* DOX), the 2.5-fold increase in survival of the nanochain-treated animals followed by RF is highly significant considering the highly invasive nature of the CNS-1 model.

To illustrate the therapeutic efficacy of the nanochain treatment, we also used the 9L model, which is an aggressive but not invasive glioma model. As expected, the therapeutic effect of the free DOX treatment was negligible as indicated by the survival time being similar to the untreated group. While 100% of the untreated and DOX-treated mice died within 28 days, 40% of the nanochain-treated group followed by RF was still alive after 77 days (Fig. 5C). At the terminal point, *post portem* measurements showed that the tumor at the primary site was 1.8±0.17 mm (mean±s.d.) in size for both animal models.

The average weight progression for each group is shown in Supplementary Fig. S5. Due to the highly selective deposition of the nanochain particles at brain tumors and the subsequent efficient spreading of drug, this significant therapeutic outcome was achieved at a very low dose (*i.e.* 0.5 mg/kg), which is 10-20-fold lower than the typical clinical regimens of liposomal DOX.

DISCUSSION

Invasive brain tumors are recognized as one of the deadliest forms of cancer. This stems from the fact that radiation therapy and surgical resection are incapable of completely removing deeply penetrating, diffuse brain tumors (1, 2). As a result, median survival is merely prolonged to 12 months following the combination of surgical resection and focal radiotherapy. At the same time, even though potent cytotoxic drugs are available to oncologists, systemic chemotherapy is not the primary treatment of choice for malignant

brain tumors due to the presence of the BTB, which limits transport to lipophilic or low molecular weight, uncharged compounds. In an effort to prevent exposure of healthy organs to the toxic side effects of chemotherapeutics and avoid having to penetrate the BTB, implantable drug depots within a brain tumor are currently being used in clinical practice (3). For example, Gliadel, an intracranial implantable biodegradable polymer loaded with the lipophilic drug BCNU, extends the median survival of patients with grade IV glioma by 13.4 weeks compared to placebo (27). On the other hand, systemic administration of nanoparticles has the potential to facilitate access to the entire brain tumor by utilizing the tumor's own blood supply.

Historically, attempts to improve nanoparticle homing to brain tumors have relied on the EPR effect followed by targeting of various receptors to direct the nanoparticle-drug complex into brain tumor cells. However, even though the BTB slightly compromises the nature of BBB, brain tumors consist of blood vessels that are not as leaky as the angiogenic vessels observed in other cancer types. This results in low penetration of nanoparticles into the brain tumor interstitium resulting in failure to reach the majority of the primary tumor mass and especially its invasive sites (6). Furthermore, the EPR effect is typically noticeable at the core regions of a brain tumor, while it is attenuated at the invasive sites of brain tumors with dispersing cancer cells. This is due to the fact that the BBB of invasive sites has a very high likelihood to remain intact. Importantly, it is not uncommon to find dispersing brain tumor cells as far away as 4 cm from the primary site (28). Along these lines, the nanochain-based therapy exploits the tumor vasculature as a docking site for the nanoparticles followed by RF-triggered drug release to spread the drug throughout the primary tumor and its invasive sites, which are nearly inaccessible by today's systemic therapeutics.

While various receptors have been exploited to target nanoparticles to cancer cells (*e.g.* folate, EGF receptors) (29-34), our work suggests that $\alpha_v\beta_3$ integrin-mediated vascular targeting provides highly selective targeting of brain tumors. In fact, the structure and shape of the nanochains have been specifically designed to target the tumor vascular bed (9). The particle shape governs the navigation of circulating nanoparticles through different biological processes, including targeting of difficult-to-reach cancer sites (35). One of the pivotal steps dictating the transport of flowing nanoparticles is their margination towards the blood vessel walls. Contrary to spherical nanoparticles, nanoparticles with geometrical asymmetry (*e.g.*, oblong shape) are subjected to torques resulting in tumbling and rotation, which increase the lateral drift of nanoparticles towards the blood vessel walls in microcirculation (36-38). Furthermore, the particle shape also governs the targeting avidity of nanoparticles using receptor-ligand systems. Compared to nanospheres, oblong-shaped nanoparticles exhibit enhanced targeting avidity due to geometrically enhanced multivalent docking. Indeed, within 24 h post-injection, integrin-targeting of nanochains resulted in a 4.7% of the administered dose being localized in brain tumor, which was 3-fold higher than integrin-targeting liposomes. Regarding the *in vivo* fate of the remaining nanochains, our previous publication evaluated the organ distribution of nanochains, which was comparable to the behavior of standard 100-nm PEGylated liposomes (7). At 24 h post-injection, the nanochains were mostly found in the reticuloendothelial organs (liver and spleen). Even

though such a significant portion of the injected dose accumulated at the tumor site, the histological studies show that no spread of DOX in the brain tumor was observed in the absence of the external stimulus (*i.e.*, RF field). Not surprisingly, even with the enhanced targeting, the nanochain treatment (without RF) provided only modest benefits in terms of prolonged survival. This is primarily related to the drug release profile from nanoparticles. While free drug in its molecular form quickly spreads within the tumor interstitium (39-41), nanoparticles, without any triggering mechanism, release their content at a relatively slow rate, once they deposit at the target site. This slow release generates a low temporal and spatial concentration gradient of the drug, resulting in non-cytotoxic levels of the drug distal from the particle (41).

While previous studies exploited vascular targeting for anti-angiogenic strategies (13, 42, 43), we coupled vascular targeting of nanochains to a unique triggered release mechanism to spread high amounts of drug into the hard-to-reach brain tumors. In a previous study (7), we assessed the relation of the nanochain's structure to RF-triggered drug release. Through their interaction with magnetic fields at the selected frequency of 10 kHz, the IO component of the nanochain particle efficiently converts magnetic energy to mechanical vibration resulting in "mechanical" disruption of the liposomal membrane. Contrary to heat-induced drug release achieved by other nanoparticle designs (*e.g.*, thermosensitive nanoparticles incorporating iron oxide or gold nanoparticles) (44), the release mechanism of nanochains results in rapid and efficient drug release even from very low concentration of nanoparticles. This ability stems from the structure of the nanochains, in such fashion that the response of the nanoparticles to the 10 kHz oscillating magnetic field is a mechanical "vibration" of the chain, rather than true rotational motion or heat dissipation (7). For example, while application of RF induced rapid release of DOX from nanochains at very low particle concentration, negligible DOX release was observed from liposomes encapsulating DOX and iron oxide nanospheres. While a nanochain containing more than 3 IO nanospheres may exhibit even faster triggered release profiles, a nanochain larger than 150 nm in length (*i.e.*, 4 or more IO nanospheres) reduces significantly the extraction yield of nanochains from the resin during the solid-phase-based synthesis of the particles. Furthermore, the RF frequencies and power used in our system are lower than those experienced in a conventional clinical MRI (*e.g.*, 64 MHz at kilowatts of power). These RF fields are well understood, and thus the design, cost and clinical deployment of such system present a low degree of difficulty.

In addition to the drug delivery barrier of gliomas, it is important to recognize that glioma cells tend to be particularly resistant to drugs. The underlying causes for the failure of therapies against brain tumors may be diverse but cellular hierarchies have been identified defined in glioblastomas with self-renewing tumor initiating cells at the apex that frequently display resistance to conventional treatments and can migrate to cause tumor recurrence (45-47). For our initial studies, we chose doxorubicin as a drug model candidate, because of its fluorescence properties and its ability to rapidly diffuse through cellular membranes and reach nuclear DNA, which functions as a sink for DOX (39-41). While it is well established that free DOX displays very poor penetration into gliomas and is nearly inaccessible to brain tumor cells (48-50), our data indicate the enormous potential of the nanochain therapeutic

strategy to deliver DOX to glioma cells. To address both challenges of drug delivery and multi-drug resistance, future studies will seek to integrate the nanochain technology with the appropriate combination of complementary drugs to enable effective treatment of the "general population" of glioma cells as well as the small fraction of glioma cells that are resistant.

In this study, we show that both the particle shape and the multicomponent nature of the nanochain particle played an essential role in its therapeutic efficacy against invasive gliomas. Coupling a vascular targeting strategy with the RF-triggered drug release of nanochains overcame the BTB issues, enabling high drug concentrations and widespread delivery within the tumor and therefore provided an increased likelihood of highly effective treatment of invasive brain cancer using a low dose of cytotoxic drugs.

Supplementary Material

Refer to Web version on PubMed Central for supplementary material.

ACKNOWLEDGEMENTS

We would like to acknowledge Dishen Lin, Swetha Rao and Samantha Tucci for help with animal studies and histology.

Financial support: This work was supported by grants from the National Cancer Institute (R01CA177716), the Clinical and Translational Science Collaborative of Cleveland (UL1TR000439) from the National Center for Advancing Translational Sciences component of the National Institutes of Health, the Case Comprehensive Cancer Center (P30CA043703), and the Ohio Cancer Research Associates (E.K.). L.B. was supported by a fellowship from the National Cancer Institute Training Program in Cancer Pharmacology (R25CA148052).

REFERENCES

1. Juratli TA, Schackert G, Krex D. Current status of local therapy in malignant gliomas--a clinical review of three selected approaches. Pharmacol Ther. 2013; 139:341–58. [PubMed: 23694764]
2. Adamson C, Kanu OO, Mehta AI, Di C, Lin N, Mattox AK, et al. Glioblastoma multiforme: a review of where we have been and where we are going. Expert opinion on investigational drugs. 2009; 18:1061–83. [PubMed: 19555299]
3. Wang PP, Frazier J, Brem J. Local drug delivery to the brain. Advanced Drug Delivery Reviews. 2002; 54:987–1013. [PubMed: 12384318]
4. Koukourakis MI, Koukouraki S, Kelekis N, Kyrias G, Karkavitsas N. High intratumoural accumulation of stealth liposomal doxorubicin (Caelyx) in glioblastomas and in metastatic brain tumours. Br J Cancer. 2000; 83:1281–6. IF. SA. [PubMed: 11044350]
5. Hobbs SK, Monsky WL, Yuan F, Roberts WG, Griffith L, Torchilin VP, et al. Regulation of transport pathways in tumor vessels: role of tumor type and microenvironment. Proc Natl Acad Sci U S A. 1998; 95:4607–12. [PubMed: 9539785]
6. Baumann BC, Kao GD, Mahmud A, Harada T, Swift J, Chapman C, et al. Enhancing the efficacy of drug-loaded nanocarriers against brain tumors by targeted radiation therapy. Oncotarget. 2013; 4:64–79. [PubMed: 23296073]
7. Peiris PM, Bauer L, Toy R, Tran E, Pansky J, Doolittle E, et al. Enhanced Delivery of Chemotherapy to Tumors Using a Multicomponent Nanochain with Radio-Frequency-Tunable Drug Release. ACS Nano. 2012; 6:4157–68. [PubMed: 22486623]
8. Peiris PM, Schmidt E, Calabrese M, Karathanasis E. Assembly of linear nano-chains from iron oxide nanospheres with asymmetric surface chemistry. PLoS One. 2011; 6:e15927. [PubMed: 21253600]

9. Peiris PM, Toy R, Doolittle E, Pansky J, Abramowski A, Tam M, et al. Imaging metastasis using an integrin-targeting chain-shaped nanoparticle. ACS Nano. 2012; 6:8783–95. [PubMed: 23005348]
10. Peiris PM, Tam M, Vicente P, Abramowski A, Toy R, Bauer L, et al. On-command drug release from nanochains inhibits growth of breast tumors. Pharm Res. 2014; 31:1460–8. [PubMed: 23934254]
11. Schnell O, Krebs B, Carlsen J, Miederer I, Goetz C, Goldbrunner RH, et al. Imaging of integrin alpha(v)beta(3) expression in patients with malignant glioma by [18F] Galacto-RGD positron emission tomography. Neuro-oncology. 2009; 11:861–70. [PubMed: 19401596]
12. Reardon DA, Nabors LB, Stupp R, Mikkelsen T. Cilengitide: an integrin-targeting arginine-glycine-aspartic acid peptide with promising activity for glioblastoma multiforme. Expert opinion on investigational drugs. 2008; 17:1225–35. [PubMed: 18616418]
13. Danhier F, Vroman B, Lecouturier N, Crokart N, Pourcelle V, Freichels H, et al. Targeting of tumor endothelium by RGD-grafted PLGA-nanoparticles loaded with paclitaxel. J Control Release. 2009; 140:166–73. [PubMed: 19699245]
14. Reddy GR, Bhojani MS, McConville P, Moody J, Moffat BA, Hall DE, et al. Vascular targeted nanoparticles for imaging and treatment of brain tumors. Clin Cancer Res. 2006; 12:6677–86. [PubMed: 17121886]
15. Bello L, Francolini M, Marthyn P, Zhang J, Carroll RS, Nikas DC, et al. Alpha(v)beta3 and alpha(v)beta5 integrin expression in glioma periphery. Neurosurgery. 2001; 49:380–9. discussion 90. [PubMed: 11504114]
16. Phuphanich S, Brat DJ, Olson JJ. Delivery systems and molecular targets of mechanism-based therapies for GBM. Expert review of neurotherapeutics. 2004; 4:649–63. [PubMed: 15853584]
17. Brooks PC, Clark RA, Cheresh DA. Requirement of vascular integrin alpha(v)beta(3) for angiogenesis. Science. 1994; 264:569–71. [PubMed: 7512751]
18. Brooks PC, Stromblad S, Klemke R, Visscher D, Sarkar FH, Cheresh DA. Anti-integrin alpha(v)beta(3) blocks human breast cancer growth and angiogenesis in human skin. J Clin Invest. 1995; 96:1815–22. [PubMed: 7560073]
19. Murphy EA, Majeti BK, Barnes LA, Makale M, Weis SM, Lutu-Fuga K, et al. Nanoparticle-mediated drug delivery to tumor vasculature suppresses metastasis. Proc Natl Acad Sci U S A. 2008; 105:9343–8. [PubMed: 18607000]
20. Kiessling F, Huppert J, Zhang C, Jayapaul J, Zwick S, Woenne EC, et al. RGD-labeled USPIO inhibits adhesion and endocytotic activity of alpha(v)beta(3)-integrin-expressing glioma cells and only accumulates in the vascular tumor compartment. Radiology. 2009; 253:462–9. [PubMed: 19789239]
21. Peiris PM, Toy R, Abramowski A, Vicente P, Tucci S, Bauer L, et al. Treatment of cancer micrometastasis using a multicomponent chain-like nanoparticle. J Control Release. 2014; 173:51–8. [PubMed: 24188960]
22. Bolotin E, Cohen R, Bar L, Emanuel N, Ninio S, Lasic D, et al. Ammonium sulfate gradients for efficient and stable remote loading of amphipathic weak bases into liposomes and ligandoliposomes. Journal of Liposome Research. 1994; 4:455–79.
23. Barth RF, Kaur B. Rat brain tumor models in experimental neuro-oncology: the C6, 9L, T9, RG2, F98, BT4C, RT-2 and CNS-1 gliomas. J Neurooncol. 2009; 94:299–312. [PubMed: 19381449]
24. Jacobs VL, Valdes PA, Hickey WF, De Leo JA. Current review of in vivo GBM rodent models: emphasis on the CNS-1 tumour model. ASN neuro. 2011; 3:e00063. [PubMed: 21740400]
25. Burden-Gulley SM, Qutaish MQ, Sullivant KE, Lu H, Wang J, Craig SE, et al. Novel cryo-imaging of the glioma tumor microenvironment reveals migration and dispersal pathways in vivid three-dimensional detail. Cancer Res. 2011; 71:5932–40. [PubMed: 21862632]
26. Karathanasis E, Chan L, Balusu SR, D'Orsi CJ, Annapragada AV, Sechopoulos I, et al. Multifunctional nanocarriers for mammographic quantification of tumor dosing and prognosis of breast cancer therapy. Biomaterials. 2008; 29:4815–22. [PubMed: 18814908]
27. Brem H, Ewend MG, Piantadosi S, Greenhoot J, Burger PC, Sisti M. The safety of interstitial chemotherapy with BCNU-loaded polymer followed by radiation therapy in the treatment of newly diagnosed malignant gliomas: phase I trial. J Neurooncol. 1995; 26:111–23. [PubMed: 8787853]

28. Iacob G, Dinca EB. Current data and strategy in glioblastoma multiforme. Journal of medicine and life. 2009; 2:386–93. [PubMed: 20108752]
29. Huang X, Peng X, Wang Y, Shin DM, El-Sayed MA, Nie S. A reexamination of active and passive tumor targeting by using rod-shaped gold nanocrystals and covalently conjugated peptide ligands. ACS Nano. 2010; 4:5887–96. [PubMed: 20863096]
30. Cheng Y, Meyers JD, Agnes RS, Doane TL, Kenney ME, Broome AM, et al. Addressing Brain Tumors with Targeted Gold Nanoparticles: A New Gold Standard for Hydrophobic Drug Delivery? Small. 2011; 7:2301–6. [PubMed: 21630446]
31. Gabizon A, Horowitz AT, Goren D, Tzemach D, Shmeeda H, Zalipsky S. In vivo fate of folate-targeted polyethylene-glycol liposomes in tumor-bearing mice. Clinical Cancer Research. 2003; 9:6551–9. [PubMed: 14695160]
32. Gabizon A, Shmeeda H, Horowitz AT, Zalipsky S. Tumor cell targeting of liposome-entrapped drugs with phospholipid-anchored folic acid-PEG conjugates. Adv Drug Deliv Rev. 2004; 56:1177–92. [PubMed: 15094214]
33. Park JW, Hong K, Kirpotin DB, Colbern G, Shalaby R, Baselga J, et al. Anti-HER2 immunoliposomes: enhanced efficacy attributable to targeted delivery. Clin Cancer Res. 2002; 8:1172–81. [PubMed: 11948130]
34. Park JW, Kirpotin DB, Hong K, Shalaby R, Shao Y, Nielsen UB, et al. Tumor targeting using anti-her2 immunoliposomes. J Control Release. 2001; 74:95–113. [PubMed: 11489487]
35. Toy R, Peiris PM, Ghaghada KB, Karathanasis E. Shaping cancer nanomedicine: the effect of particle shape on the in vivo journey of nanoparticles. Nanomedicine (Lond). 2014; 9:121–34. [PubMed: 24354814]
36. Gavze E, Shapiro M. Motion of inertial spheroidal particles in a shear flow near a solid wall with special application to aerosol transport in microgravity. Journal of Fluid Mechanics. 1998; 371:59–79.
37. Lee SY, Ferrari M, Decuzzi P. Shaping nano-/micro-particles for enhanced vascular interaction in laminar flows. Nanotechnology. 2009; 20 495101 (11pp).
38. Gentile F, Chiappini C, Fine D, Bhavane RC, Peluccio MS, Cheng MM, et al. The effect of shape on the margination dynamics of non-neutrally buoyant particles in two-dimensional shear flows. J Biomech. 2008; 41:2312–8. [PubMed: 18571181]
39. Terasaki T, Iga T, Sugiyama Y, Sawada Y, Hanano M. Nuclear binding as a determinant of tissue distribution of adriamycin, daunomycin, adriamycinol, daunorubicinol and actinomycin D. J Pharmacobiodyn. 1984; 7:269–77. [PubMed: 6470925]
40. Marafino BJ Jr. Giri SN, Siegel DM. Pharmacokinetics, covalent binding and subcellular distribution of [3H]doxorubicin after intravenous administration in the mouse. J Pharmacol Exp Ther. 1981; 216:55–61. [PubMed: 7452508]
41. Laginha KM, Verwoert S, Charrois GJ, Allen TM. Determination of doxorubicin levels in whole tumor and tumor nuclei in murine breast cancer tumors. Clin Cancer Res. 2005; 11:6944–9. [PubMed: 16203786]
42. Park JH, Kwon S, Nam JO, Park RW, Chung H, Seo SB, et al. Self-assembled nanoparticles based on glycol chitosan bearing 5beta-cholanic acid for RGD peptide delivery. J Control Release. 2004; 95:579–88. [PubMed: 15023468]
43. Nam JO, Kim JE, Jeong HW, Lee SJ, Lee BH, Choi JY, et al. Identification of the alphavbeta3 integrin-interacting motif of betaig-h3 and its anti-angiogenic effect. J Biol Chem. 2003; 278:25902–9. [PubMed: 12704192]
44. Brazel CS. Magnetothermally-responsive nanomaterials: combining magnetic nanostructures and thermally-sensitive polymers for triggered drug release. Pharm Res. 2009; 26:644–56. [PubMed: 19005741]
45. Bao S, Wu Q, McLendon RE, Hao Y, Shi Q, Hjelmeland AB, et al. Glioma stem cells promote radioresistance by preferential activation of the DNA damage response. Nature. 2006; 444:756–60. [PubMed: 17051156]
46. Singh SK, Clarke ID, Terasaki M, Bonn VE, Hawkins C, Squire J, et al. Identification of a cancer stem cell in human brain tumors. Cancer Res. 2003; 63:5821–8. [PubMed: 14522905]

47. Cheng L, Bao S, Rich JN. Potential therapeutic implications of cancer stem cells in glioblastoma. Biochemical pharmacology. 2010; 80:654–65. [PubMed: 20457135]

48. Ohnishi T, Tamai I, Sakanaka K, Sakata A, Yamashima T, Yamashita J, et al. In vivo and in vitro evidence for ATP-dependency of P-glycoprotein-mediated efflux of doxorubicin at the blood-brain barrier. Biochemical pharmacology. 1995; 49:1541–4. [PubMed: 7763297]

49. Mankhetkorn S, Dubru F, Hesschenbrouck J, Fiallo M, Garnier-Suillerot A. Relation among the resistance factor, kinetics of uptake, and kinetics of the P-glycoprotein-mediated efflux of doxorubicin, daunorubicin, 8-(S)-fluoroidarubicin, and idarubicin in multidrug-resistant K562 cells. Molecular pharmacology. 1996; 49:532–9. [PubMed: 8643093]

50. Rousselle C, Clair P, Lefauconnier JM, Kaczorek M, Scherrmann JM, Temsamani J. New advances in the transport of doxorubicin through the blood-brain barrier by a peptide vector-mediated strategy. Molecular pharmacology. 2000; 57:679–86. [PubMed: 10727512]

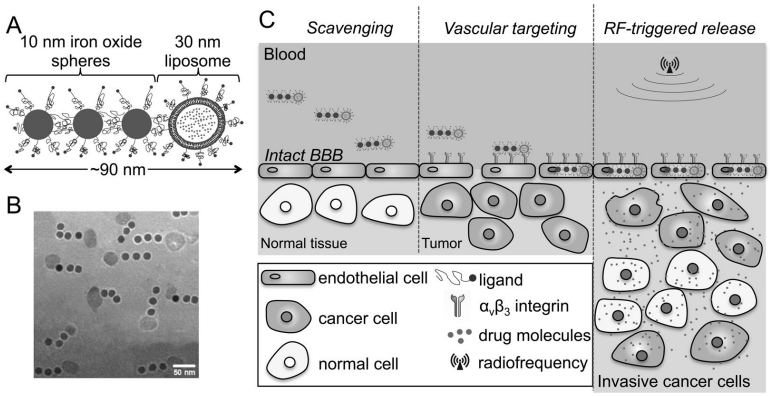

Fig. 1.

Illustration of the nanochain particle and its therapeutic effect on brain tumors. A, schematic of a linear nanochain particle composed of three IO nanospheres and one drug-loaded liposome. B, TEM image of nanochain particles. C, illustration of the successful delivery of nanochain-based drug to invasive brain cancer via vascular targeting and RF-triggered drug release.

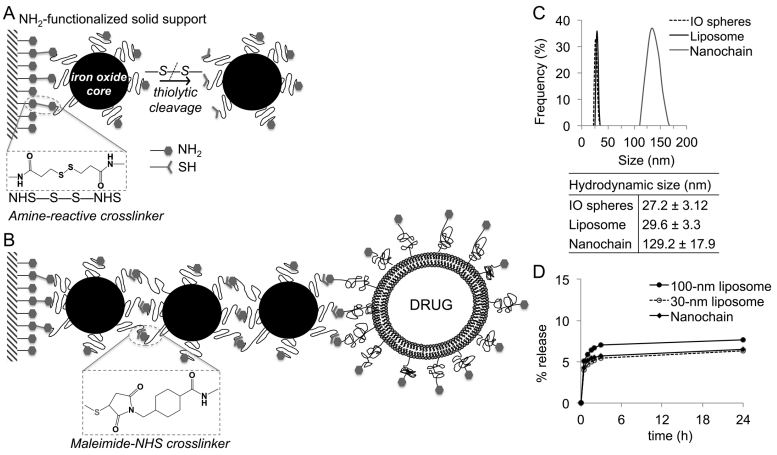

Fig. 2.

Reaction scheme of the controlled assembly of nanochains using solid-phase chemistry. A, in the first step, chemical bifunctionality on the surface of parent IO nanospheres is topologically controlled resulting in nanospheres with two faces, one displaying only amines and the other only thiols. B, in the second step, the two unique faces on the parent nanosphere serve as fittings to chemically assemble them into nanochains. C, size distribution of nanochain particles and their parent nanospheres obtained by DLS (data presented as mean ± s.d.). D, comparison of *in vivo* blood plasma stability of nanochains to 30-nm and 100-nm liposomal DOX. In a typical leakage procedure, 1 mL of formulation was placed in dialysis tubing with 100k MWCO and dialyzed against blood plasma at 37°C.

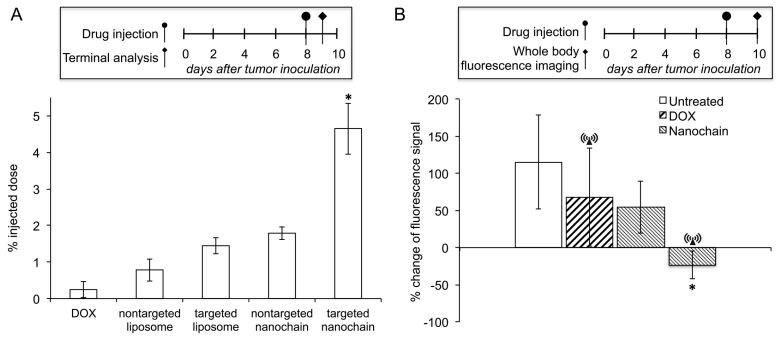

Fig. 3.

Evaluation of the ability of nanochains to target invasive brain tumors in mice. A, CNS-1 cells (2×10^5) were implanted in the right striatum at a depth of 3 mm from dura. At 8 days after tumor inoculation, the animals were injected with DOX, non-targeted liposomes, integrin-targeting liposomes, non-targeted nanochains and targeted nanochains. All formulations were administered at a dose 0.5 mg DOX per kg of body weight (n=4 mice per group; * $P<0.01$ by Student's t-test). At 24 h after injection, animals were euthanized, brain tumors were excised and their DOX content was extracted and measured using an established method. B, as a metric of the response of brain tumors to various treatments (n=5 in each group), quantification of fluorescence intensity (FI) was used. The stable expression of green fluorescence protein within the CNS-1 cells enabled *in vivo* imaging using a CRi Maestro fluorescence imaging system. All formulations were administered at day 8 after tumor inoculation at a dose of 0.5 mg DOX per kg b.w. In the case of treatments combined with the RF field, animals were exposed for 60 min to an RF field (amplitude B=5 mT, frequency f=10 kHz) using a custom-made solenoid coil. The y-axis represents the normalized difference of fluorescence signal between days 8 and 10 (calculation of normalized value $[(FI^{day8}- FI^{day10})/FI^{day8}]x100$; n=5 in each group; * $P<0.01$ by Student's t-test)

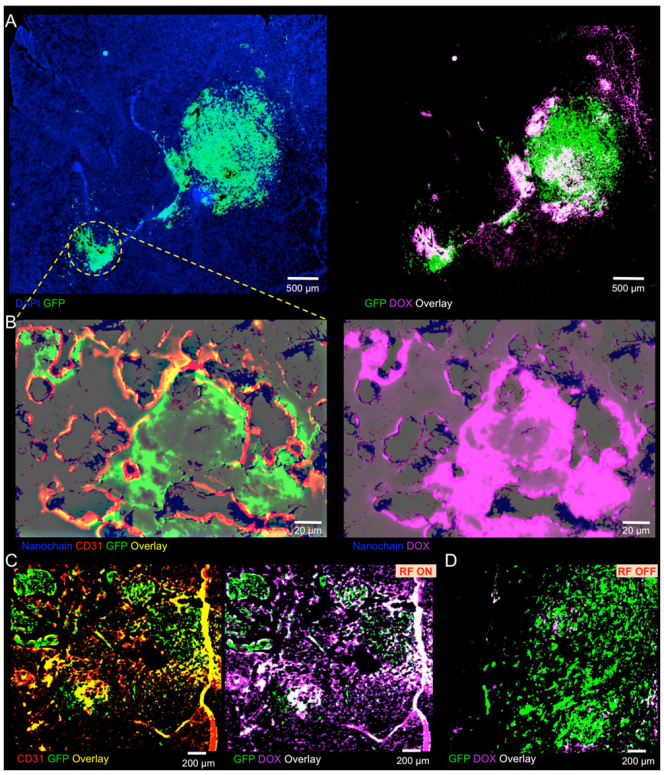

Fig. 4.

Histological evaluation of the nanochain treatment. A, histological evaluation of the anticancer effect of nanochains was performed in the orthotopic CNS-1 model in mice (5x magnification; green: CNS-1 glioma cells (GFP); blue: nuclear stain (DAPI); violet: DOX). Fluorescence imaging of an entire histological section of the brain shows the primary tumor and its invasive sites (left panel). Fluorescence imaging of the same histological section shows the widespread distribution of DOX molecules after a 60-min application of RF (right panel). B, higher magnification imaging (20x) of an invasive site shows the location of nanochains (blue) with respect to the location of endothelial cells (green: CD 31) and brain tumor cells (left panel), and the RF-triggered release of DOX (right panel) in the same histological section. Nanochains were visualized by staining iron with Prussian blue. The distribution of DOX molecules is shown with (C) or without RF (D) with respect to the location of cancer cells.

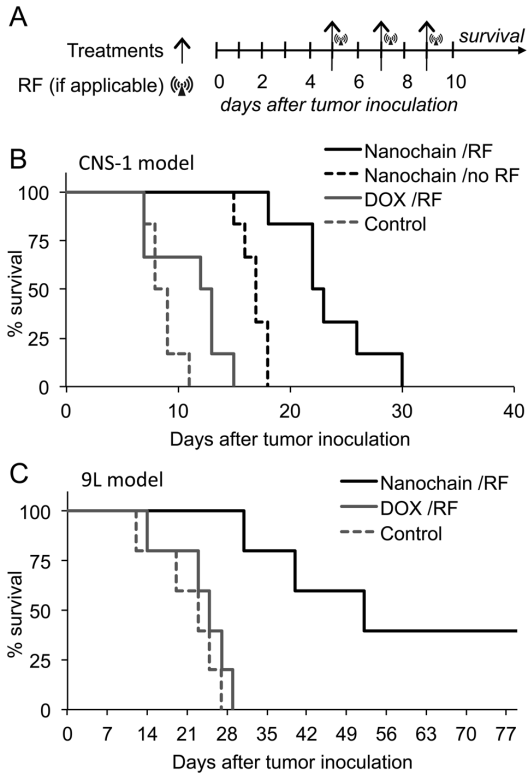

Fig. 5.

Treatment of brain tumor using nanochains. A, the schedule of treatments and application of RF are shown with respect to tumor inoculation. All formulations were administered at a dose of 0.5 mg DOX per kg b.w. Each treatment was administered three times at day 5, 7 and 9 after tumor inoculation. In the case of treatments combined with the RF field, animals were exposed for 60 min to an RF field (amplitude B=5 mT, frequency f=10 kHz) using a custom-made solenoid coil. B, the survival times of CNS-1 tumor-bearing animals are shown after treatment with saline (untreated group), DOX followed by RF, nanochains (no RF), and nanochains followed by RF (n=5 mice in each group). C, the survival times of 9L tumor-bearing animals are shown after treatment with saline (untreated group), DOX followed by RF, and nanochains followed by RF (n=5 mice in each group).